



Electronic Retinal Prostheses

Daniel Palanker

Department of Ophthalmology and Hansen Experimental Physics Laboratory, Stanford University, Stanford, California 94305, USA

Correspondence: palanker@stanford.edu

Retinal prostheses are a promising means for restoring sight to patients blinded by photoreceptor atrophy. They introduce visual information by electrical stimulation of the surviving inner retinal neurons. Subretinal implants target the graded-response secondary neurons, primarily the bipolar cells, which then transfer the information to the ganglion cells via the retinal neural network. Therefore, many features of natural retinal signal processing can be preserved in this approach if the inner retinal network is retained. Epiretinal implants stimulate primarily the ganglion cells, and hence should encode the visual information in spiking patterns, which, ideally, should match the target cell types. Currently, subretinal arrays are being developed primarily for restoration of central vision in patients impaired by age-related macular degeneration (AMD), while epiretinal implants—for patients blinded by retinitis pigmentosa, where the inner retina is less preserved. This review describes the concepts and technologies, preclinical characterization of prosthetic vision and clinical outcomes, and provides a glimpse into future developments.

Retinal degenerative diseases are among the leading causes of incurable blindness today (Smith et al. 2001). While photoreceptors are lost in retinal degeneration, the inner retinal neurons survive to a large extent (Humayun et al. 1999; Kim et al. 2002; Mazzoni et al. 2008), providing an opportunity to reintroduce visual information into the neural system by electrical stimulation of the remaining neurons.

Photoreceptors (about 100 million in a human eye) hyperpolarize upon illumination, which, in turn, reduces the glutamate release rate in synapses with about a dozen types of bipolar cells (BCs). Two types of horizontal cells modulate these synapses, providing edge enhancement and some aspects of the contrast adaptation. BCs (about 10 million in total) are also

graded-response neurons, which integrate visual information from multiple photoreceptors and relay it to about two dozen types of retinal ganglion cells (RGCs, about one million), which generate the action potentials propagating to the brain (Fig. 1A,B). About 30 types of amacrine cells (Masland 2001; Wässle 2004) regulate the synapses between BCs and ganglion cells, providing various aspects of spatiotemporal filtering. Different types of RGCs encode various aspects of the visual information in a plurality of ways, including increments or decrements of light (ON and OFF cells), color opponency (blue-yellow, red-green) (Field et al. 2007), various sizes of receptive fields (midget and parasol), segregation of the object motion from that of a background (Olveczky et al. 2003), and many others.

Editors: Eyal Banin, Jean Bennett, Jacque L. Duncan, Botond Roska, and José-Alain Sahel
Additional Perspectives on Retinal Disorders: Genetic Approaches to Diagnosis and Treatment available at
www.perspectivesinmedicine.org

Copyright © 2023 Cold Spring Harbor Laboratory Press; all rights reserved
Advanced Online Article. Cite this article as *Cold Spring Harb Perspect Med* doi: 10.1101/cshperspect.a041525

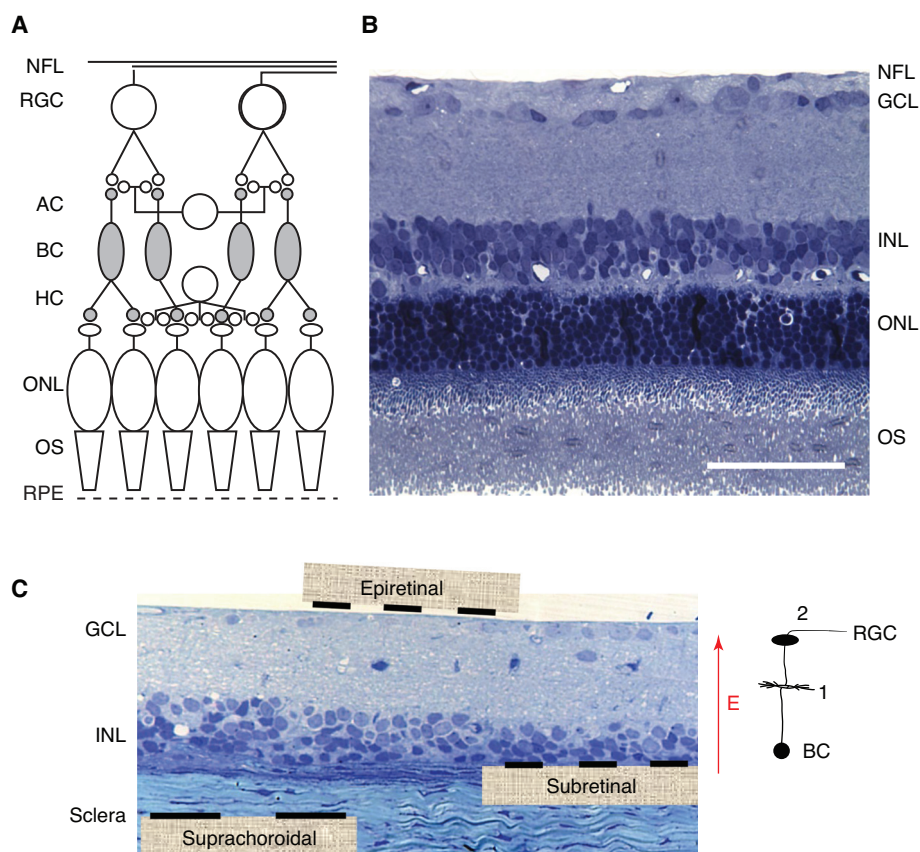


Figure 1. Retina and the implant placement. (A) Diagrammatic view of the retinal wiring. Signals from the photoreceptors (including the nuclei in the outer nuclear layer [ONL] and the outer segments [OS]) are processed by the second-order neurons (horizontal [HCs] and bipolar cells [BCs], located in the inner nuclear layer [INL]) and relayed to the third-order neurons—the retinal ganglion cells (RGCs) regulated by the amacrine cells (ACs). The RGC axons in the nerve fiber layer (NFL) transmit the visual signals to the brain. Photoreceptor OS are in contact with the retinal pigment epithelium (RPE). (B) Histology of a healthy rat retina. Scale bar, 50 μm . (C) Histology of a degenerate rat retina (RCS). Epiretinal implants are placed above the nerve fiber layer. Subretinal implants are placed below the INL instead of the missing photoreceptors. Suprachoroidal implants are inserted into the sclera below the choroid. (GCL) Ganglion cell layer.

Age-related macular degeneration (AMD) is a leading cause of untreatable vision loss, affecting over 8.7% of the population worldwide (Wong et al. 2014). Advanced forms of AMD are associated with severe visual impairment, and their prevalence dramatically increases with age: from 1.5% above 40 yr to more than 15% in populations older than 80 in the United States (Friedman et al. 2004). The dry form of advanced AMD, called geographic atrophy (GA), is associated with a loss of photoreceptors in the center of the macula. Since human visual

acuity decreases with eccentricity (Wandell 1995), loss of high-resolution central vision severely impairs reading and face recognition, while the low-resolution peripheral vision still allows for normal ambulation. Therefore, restoration of central vision in such conditions should provide sufficiently high acuity for reading and face recognition, without jeopardizing the surrounding peripheral retina.

Retinitis pigmentosa (RP) is a broad class of genetic disorders, which typically affects relatively young patients (in their twenties or thir-

ties), with an incidence rate of approximately 1:4000 (Haim 2002). This inherited disease typically begins with a loss of rod photoreceptors in the mid-periphery, that gradually expands toward the peripheral retina and toward the fovea, eventually leading to blindness due to loss of the cone photoreceptors in the central retina. For these patients, independent ambulation would already be a great benefit, even if resolution of prosthetic vision would not suffice for reading.

While retinal degenerations leave the number of the inner retinal neurons (inner nuclear layers [INLs] and ganglion cell layers [GCLs]) relatively intact for an extended period of time (Humayun et al. 1999; Kim et al. 2002), significant changes in wiring of the retinal network can take place at the end phases of the disease, when the vast majority of the photoreceptors are lost (Marc and Jones 2003; Marc et al. 2003; Jones and Marc 2005). During retinal remodeling, amacrine and BCs can migrate either to the distal retina or to the GCL. In the final stages of the retinal remodeling, neuronal death can also significantly deplete the INL and GCL, with glial cells partially filling the space left by deceased neurons (Marc and Jones 2003; Marc et al. 2003). Spontaneous firing patterns of RGCs change significantly with degeneration (Margolis et al. 2008; Menzler and Zeck 2011; Sekirnjak et al. 2011), and electrical stimulation thresholds of certain types of RGCs can increase (Cho et al. 2016).

AMD patients are less likely to suffer from extensive retinal remodeling compared to RP since (1) the peripheral retina is preserved, which helps in maintaining more normal neural activity in the center via lateral connectivity in the retinal network, and (2) the onset of the disease is much later in life and hence its duration is shorter. However, even in such a local retinal degeneration, the RGC spiking rate may increase significantly (Tochitsky et al. 2014).

ELECTRICAL STIMULATION OF NEURONS

Neural activity can be affected by modulating the cell potential with electric current. Extracellular stimulation works by polarizing the cells in an

electric field: since the cell membrane is highly resistive while its cytoplasm is very conductive, electric fields in extracellular medium redistribute the charges along the cell membrane such that the cytoplasm rapidly (sub- μ s in cell soma) becomes equipotential (Boinagrov et al. 2010). As a result, the transmembrane potential step increases (i.e., the membrane is hyperpolarized) on the side of the cell facing the anode and decreases (the membrane is depolarized) on the opposite side. When the membrane potential exceeds a certain threshold (typically around 10 mV [Boinagrov et al. 2010]) on a depolarized side, the voltage-gated ion channels open, increasing the influx of positive ions (Na^+ in ganglion cells, Ca^{2+} in BCs), resulting in cellular depolarization as a whole. This, in turn, may lead to generation of the action potential in spiking cells (RGCs), or just increase in the neurotransmitter release rate from axonal terminals in the graded-response cells (BCs).

Since the distribution of ion channels over neurons is typically anisotropic, orientation of the electric field significantly affects the stimulation threshold. It is lower when the side of a cell with the highest concentration of the responding ion channels is depolarized. Therefore, the pulse polarity (anodic or cathodic), as well as placement of the stimulating electrode (above or below the retina—epiretinal or subretinal), affects the stimulation threshold. For epiretinal stimulation of RGCs, cathodic-first pulses have a lower stimulation threshold than anodic (Jensen et al. 2005; Fried et al. 2006; Boinagrov et al. 2014) due to a higher concentration of Na voltage-sensitive ion channels near the axon initial segment (Fried et al. 2006). For subretinal stimulation of RGCs, anodic-first pulses have lower stimulation thresholds for the same reason (Jensen and Rizzo 2006; Boinagrov et al. 2014). Similarly, for subretinal stimulation of the BCs in the INL, anodic pulses have a lower threshold (Boinagrov et al. 2014) because of higher concentration of the voltage-sensitive Ca channels in BC's axonal terminals (Werginz et al. 2015). For small electrodes, proximity to the target neuron is another factor that significantly affects the stimulation threshold, since in this case the electric potential rapidly decreases with distance. A combination

D. Palanker

of a good placement of the stimulating electrode and a proper choice of the stimulation parameters can help achieve selective activation of various retinal neurons (Boinagrov et al. 2014).

Epiretinal prostheses aim at eliciting RGC response directly. Since the Na ion channels underlying the RGC stimulation are much faster than the Ca channels responsible for BC response, RGCs have shorter chronaxie (around 1 msec) than BCs (around 3–4 msec), so the stimulation threshold continues to decrease with increasing pulse duration at least to 20 msec. The strength–duration relationships of the stimulation thresholds for direct and network-mediated responses demonstrated that short (<1 msec) cathodic-first pulses from an epiretinal electrode provide the best RGC/BC selectivity of about a factor of 3 (Boinagrov et al. 2014). Conversely, subretinal anodic-first pulses provide higher selectivity for BCs using longer stimuli, exceeding a factor of 6 for 20 msec pulses (Boinagrov et al. 2014).

Relative position of the active and return electrodes in the implant affects the cross talk between neighboring pixels, and thereby can also affect the contrast, selectivity, and attainable resolution (Palanker et al. 2005; Loudin et al. 2007; Flores et al. 2016). Many implants operate with a remote return electrode in the so-called monopolar configuration. Cross talk between the neighboring pixels increases with a larger number of simultaneously activated electrodes. To overcome this limitation, local return electrodes can be placed around each stimulating electrode (Loudin et al. 2007; Mathieson et al. 2012). However, local returns decrease the electric field penetration depth, compared to a monopolar configuration, and thus impose more stringent limits on distance between the stimulating electrodes and the target neurons. This has led to development of three-dimensional implants (Ho et al. 2019) and current steering approaches (Chen et al. 2020) to optimize the field shaping.

In cell somas, membrane polarization is defined largely by the voltage step across the cell boundaries (i.e., by the integral of the electric field along the cell length). Axons are modeled as leaky cables, where the activating function is

defined by the derivative of the electric field along the axon (Malmivuo and Plonsey 1995). Unfortunately, RGC stimulation with epiretinal electrodes is primarily axonal, making the selective and local activation of RGCs rather difficult to achieve (Nanduri et al. 2012; Grosberg et al. 2017).

APPROACHES TO RETINAL PROSTHETICS

Anatomical Placement and the Target Cells

Depending on their location in patient's eye, retinal implants are categorized as epiretinal, subretinal, or suprachoroidal (Fig. 1C).

Epiretinal Implants

In the “epiretinal” approach, electrodes are placed on top of the inner limiting membrane, targeting primarily the RGCs (Fig. 1C; Ahuja et al. 2011; Humayun et al. 2012). Epiretinal stimulation is less dependent on the health of the inner retinal neurons and can operate as long as the RGCs are alive. Since the action potential is a binary response, modulating the stimulus amplitude, or duration above the threshold does not affect the amplitude of the elicited spike, and hence a more appropriate modulation strategy for RGCs is by controlling the stimulation timing, frequency, and burst duration. RGCs can generally respond to stimuli at frequencies of at least 100 Hz (Sekirnjak et al. 2006; Cai et al. 2011), thus enabling generation of naturalistic spike trains by direct electrical activation (Jepson et al. 2014).

A major issue with epiretinal activation of RGCs is axonal stimulation (Weitz et al. 2015; Grosberg et al. 2017). Even though the RGC stimulation threshold at the axon initial segment can be three times lower than the axonal threshold (Werginz et al. 2020), axons from distant cells in the nerve fiber layer, passing between the stimulating electrodes and the ganglion cells, may get activated, resulting in arcuate visual percepts (Nanduri et al. 2012). This effect, leading to distortion of the retinotopic map, remains a major hurdle for epiretinal implants. One approach for circumventing the problem of axonal stimu-

lation is based on the use of much longer (>20 msec) pulses to stimulate the bipolar rather than ganglion cells (Weitz et al. 2015). Doing so significantly improved the localization of phosphenes in patients; however, it precludes encoding the retinal output by direct stimulation of RGCs at high frequencies. Another approach is based on careful measurements of the local stimulation threshold under each electrode using a bidirectional implant and avoiding the electrodes that activate remote cells (Shah et al. 2019). Epiretinal implants that aim at restoring the natural visual code in specific types of RGCs (Fried et al. 2006; Jepson et al. 2014) should activate individual neurons without affecting the surrounding cells. Different RGC types were found to have somewhat different activation thresholds (Fried et al. 2009), likely due to differences in the Na channels and other anatomical or physiological properties. However, selective activation of RGCs is quite challenging: only ~7% of cells could be activated selectively even in the peripheral primate retina (Grosberg et al. 2017), while in the central macula it is even harder due to multilayered RGCs and denser axonal bundles.

Another challenge with direct encoding of the proper spiking patterns in various RGCs is identification of the cell types in the degenerate retina (Chichilnisky and Kalmar 2002). Instead of light responses, proposed cell classification is based on electrical signatures of the RGC spontaneous activity, including their electrophysiological images and autocorrelation functions (Richard et al. 2015). Applicability of this method to a degenerate retina, where spontaneous firing patterns become abnormal, remains to be tested. Another issue with an abnormally high spontaneous firing rate of RGCs frequently observed in animal models of retinal degeneration (Sekirnjak et al. 2011) is that it may diminish the corresponding perception or impede the ability of the implant to encode a desired spikes sequence.

Typically, implantation of the epiretinal devices involves vitrectomy and attachment of the implant to the retina using retinal tacks. In some epiretinal implants, such as Argus, antennae and data processors are placed outside the eyeball, under the conjunctiva, connected to the intra-

ocular part by a transscleral cable (da Cruz et al. 2013).

Subretinal Implants

In the “subretinal” approach, arrays of electrodes placed between the pigment epithelium and the INL replace the degenerated photoreceptors and target primarily the surviving BCs (Fig. 1C; Zrenner et al. 2011; Lorach et al. 2015). In nonspiking neurons, stronger stimuli can be encoded with higher amplitude or longer pulses. Output signals from BCs are then transmitted via synapses to RGCs, which convert them into the action potential trains. This approach retains some of the remaining signal-processing properties of the retinal network, and hence the spiking patterns elicited in RGCs resemble those observed in normal retina. However, changes in the retinal network during degeneration may impact the retinal signal processing, and therefore alter the encoding of the visual information. To elicit a steady percept using pulsatile stimulation, its frequency should exceed that of flicker fusion (Lorach et al. 2015; Ho et al. 2019; Palanker et al. 2020). In BCs, this occurs at frequencies exceeding ~30–60 Hz due to accumulation of Ca in the axonal terminals and due to temporal filtering properties of the glutamate vesicles release (Werginz et al. 2020).

Implantation of the subretinal arrays in human patients involves formation of a local retinal detachment induced by subretinal injection of fluid, followed by a small retinal incision through which the device is inserted into the subretinal space, ending with the retinal reattachment (Palanker et al. 2020). In the case of wired subretinal implants, large areas of the retina are typically detached during implantation, which is a significant challenge with fragile diseased retinas. Excessively traumatic implantations can lead to fibrosis and scarring.

In a “suprachoroidal” approach, the device is inserted into the sclera below the choroid (Fig. 1C). While this approach is assumed to be surgically less risky than the epi- and subretinal prostheses (Fujikado et al. 2011; Ayton et al. 2014), the larger distance between the stimulating electrodes and the target neurons greatly

limits the attainable selectivity of retinal stimulation and the spatial resolution. Therefore, such implants have large (~ 1 mm) electrodes and are placed in the periphery of the visual field to help with low-resolution tasks, primarily for ambulation (Kolic et al. 2020).

Delivery of Power and Data to the Implant

Transmission of power and data to the implant is an engineering challenge since direct transcutaneous wiring of an implant to external electronics is prone to infections and severe scarring (Knutson et al. 2002). Therefore, transfer of power and information to modern implants is done wirelessly, using the following approaches: (1) delivery of data and power through radiofrequency (RF) coils, (2) optical delivery of data with power transmission through RF coils, or (3) optical transmission of data and power to the implant.

Several retinal implant systems use serial telemetry for data transmission: the Argus II (Second Sight Medical Systems, Sylmar, CA), shown in Figure 2, IRIS II (Hornig et al. 2017), a suprachoroidal device (Ayton et al. 2014), and the Boston Retinal Implant (Rizzo et al. 2011). Increasing the number of electrodes to thousands in the coil-based designs is rather difficult since (1) it requires a very wide bandwidth, and (2) wiring of a large number of electrodes makes the feed-through connector rather bulky and the cable quite rigid. Multiplexing the signals on the retinal implant itself would reduce the required number of wires, but it adds electronics to the implant, which affects its heating, weight, size, and flexibility.

Another option is transmission of power via RF coils, and the data—via a serial optical link from the glasses to the implant—as was done in the IRIS II system (Pixium Vision, Paris, France)

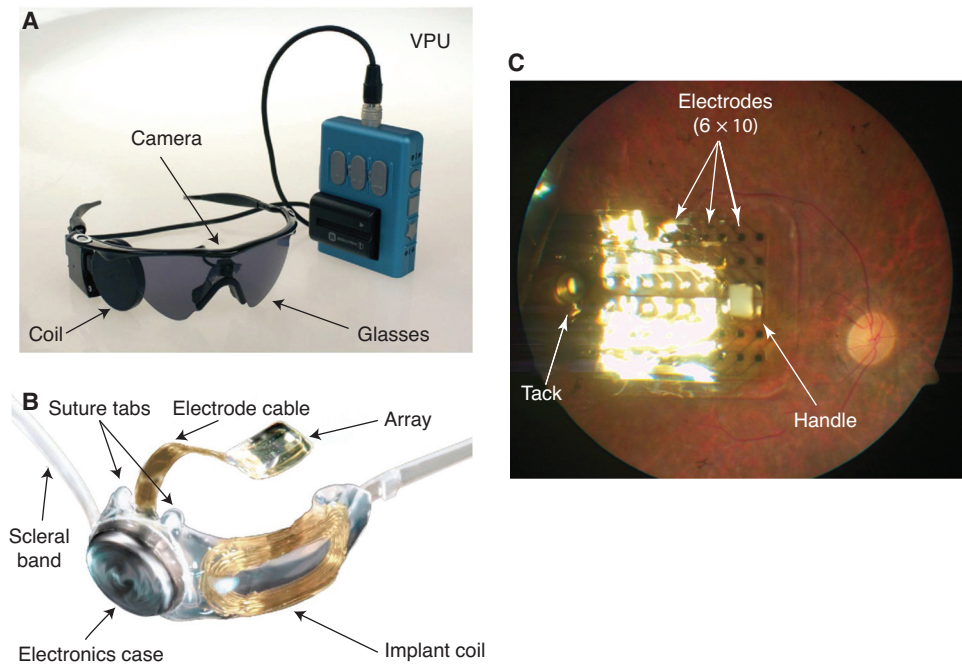


Figure 2. The Argus II epiretinal system. (A) External portion of the Argus II, including glasses with a video camera, radiofrequency (RF) coil, and a video processing unit (VPU). (B) The implantable portion of Argus II, including the implant RF coil, the electronics case, and the electrode array. (C) Fundus photo of an Argus II implant in the macula. A retinal tack attaches the electrode array to the sclera. A white handle is used for positioning the device in the eye. (All figure panels are reprinted from Humayun et al. 2012, with permission from Elsevier © 2012.)

(Hornig et al. 2017). Since the optical data-transmission rate is typically much higher than with RF, more information can be delivered to the implant.

In both approaches, the visual information is transmitted to the implant via serial telemetry, and hence it does not depend on eye movements. Since the brain expects images to shift on the retina with eye movements, static patterns with such retinal implants are perceived as moving objects. Similar phenomena have been reported with cortical visual prostheses (Naumann 2012). To avoid this effect, patients are asked to keep their gaze steady and scan the visual field with the head-mounted cameras—a very unnatural paradigm. Such problems can be alleviated by incorporating an eye tracking, which can shift the images on the implant according to the direction of gaze (Caspi et al. 2018).

A few designs have been proposed for power delivery through RF coupling and transmission of the visual information through the eye optics (Woodburn et al. 2002; Loudin et al. 2007; Zrenner et al. 2011; Ha et al. 2016). The best known was the Alpha IMS/AMS (Retina Implant AG, Reutlingen, Germany) shown in Figure 3. The subretinal implant includes photodiodes with amplifiers and stimulating electrodes in each pixel, which convert the incident images into electrical current flowing through the retina. Such optical implants naturally couple the eye movements to the stimulation pattern on the implant. The subdermal power-receiving coil with electronics placed behind the ear was connected to the subretinal implant via a transscleral cable (Stingl et al. 2017), which makes the implantation procedure difficult and prone to complications, and the feedthrough connector to the moving implant remains a challenging engineering problem (Daschner et al. 2017).

The third category of retinal implants receives both the power and data by light, via natural eye optics (Fig. 4; Mathieson et al. 2012; Ghezzi et al. 2013). Such photovoltaic implants directly convert incident light into electric current to stimulate the nearby neurons (Palanker et al. 2005; Mathieson et al. 2012; Lorach et al. 2015). To provide sufficient current for retinal

stimulation, intense illumination is projected from a near-the-eye display (Goetz et al. 2013). To avoid the photophobic and phototoxic effects of bright light, invisible near-infrared (880–915 nm) wavelengths are used. Instead of silicon photodiodes, photovoltaic elements based on light-sensitive polymers have also been proposed (Ghezzi et al. 2013). Since photovoltaic systems do not require cables (Mathieson et al. 2012; Lorach et al. 2015), the implantation procedure is greatly simplified. Implants can be composed of several modules to tile the visual field. These modules can be inserted into the subretinal space via a smaller incision and follow the eye curvature, making the surgery less traumatic than with a single larger implant (Lee et al. 2016).

PRECLINICAL EVALUATION OF PROSTHETIC VISION

Retinal Response to Electric Stimulation

Electric Receptive Fields

RGC receptive fields characterize the spatial extent sampled by individual ganglion cells. With prosthetic stimulation, it characterizes the combined point spread function of the implant and of the retinal neural network (Sim et al. 2014; Lorach et al. 2015). Spatiotemporal properties of RGCs can be assessed from the spike-triggered average responses to various stimuli in healthy and degenerate retina using a multielectrode array *ex vivo* (Ho et al. 2018a). The average photovoltaic receptive field size with 70 μm pixels was found to be similar to that of the natural visual responses: 191 μm versus 228 μm , respectively (Fig. 5A,B). Both the natural and photovoltaic receptive fields in healthy retina had an antagonistic center-surround organization (Ho et al. 2018a). In healthy retina, ON RGCs exhibited photovoltaic OFF responses, and vice versa (Fig. 5A,B). This reversal is consistent with depolarization of the photoreceptor terminals by subretinal anodic stimuli, as opposed to their hyperpolarization under light. In the degenerate rat retina, both ON and OFF photovoltaic responses were also observed: ON—primarily in RGCs with low spontaneous firing rate and OFF—in

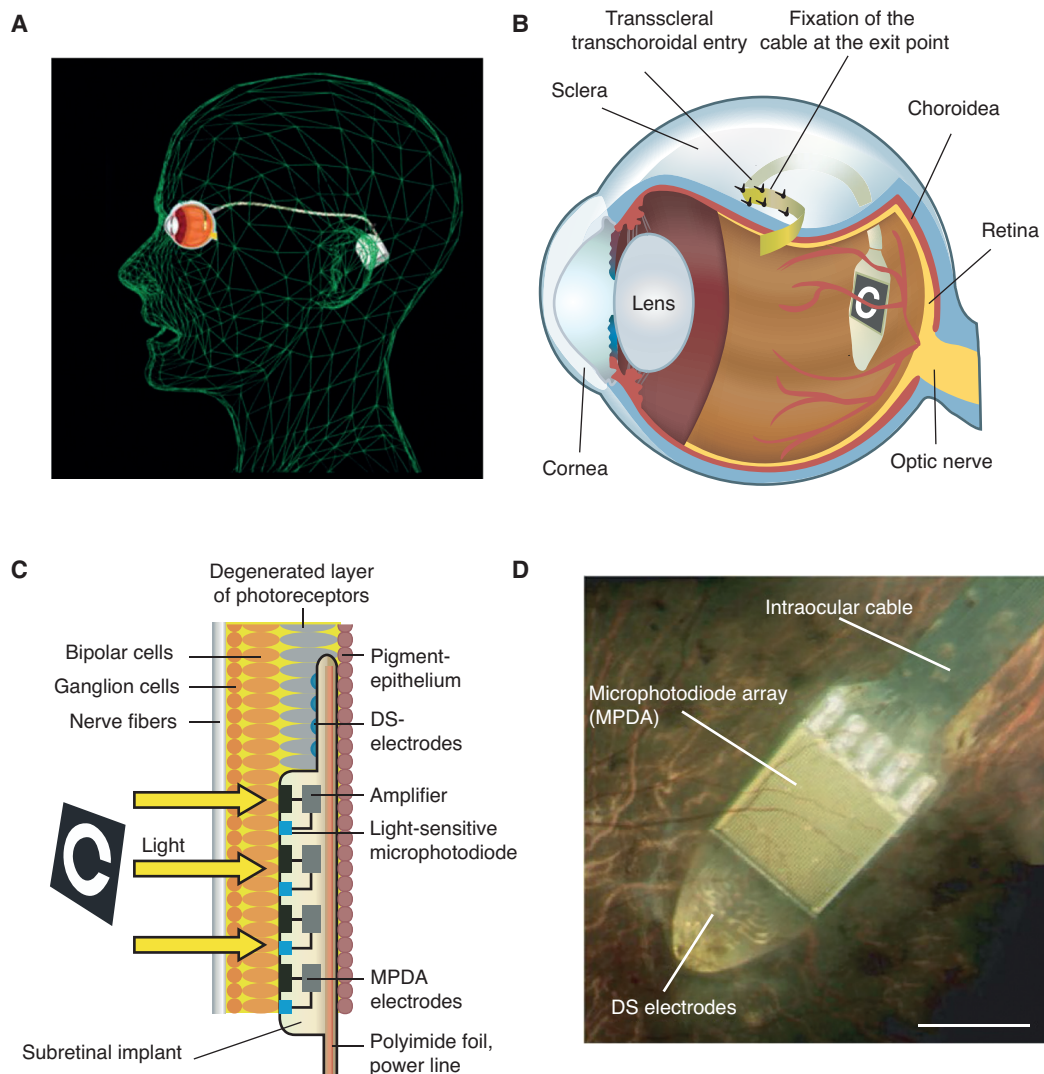


Figure 3. The Alpha IMS subretinal system. (A) A cable from the radiofrequency (RF) receiver implanted behind the ear runs under the temporal muscle, through the sclera, to the implanted chip under the retina. (B) A power cable from the implant exits the eye 3 mm behind the limbus. (C) Pixels with photodiodes, amplifiers, and electrodes are located between the pigment epithelium and the inner nuclear layer. (D) View of the subretinal implant through a pupil. Scale bar, 3 mm, corresponding to 10° of the visual angle. (Panels B, C, and D reprinted from Zrenner et al. 2011 under the terms of the Creative Commons Attribution License.)

cells with high spontaneous firing (Ho et al. 2018b). Despite the disconnected horizontal cells, the degenerate retina maintained the antagonistic center-surround organization of the receptive fields under electrical stimulation, most likely due to lateral inhibition by amacrine cells, as in healthy retina (Fig. 5C,D).

Lateral Resolution

One of the most important characteristics of vision in general and of prosthetic sight, in particular, is the visual acuity. In healthy rats, visual acuity is approximately 1 cpd (cycle per degree), which corresponds to about $28 \mu\text{m}$ on the retina

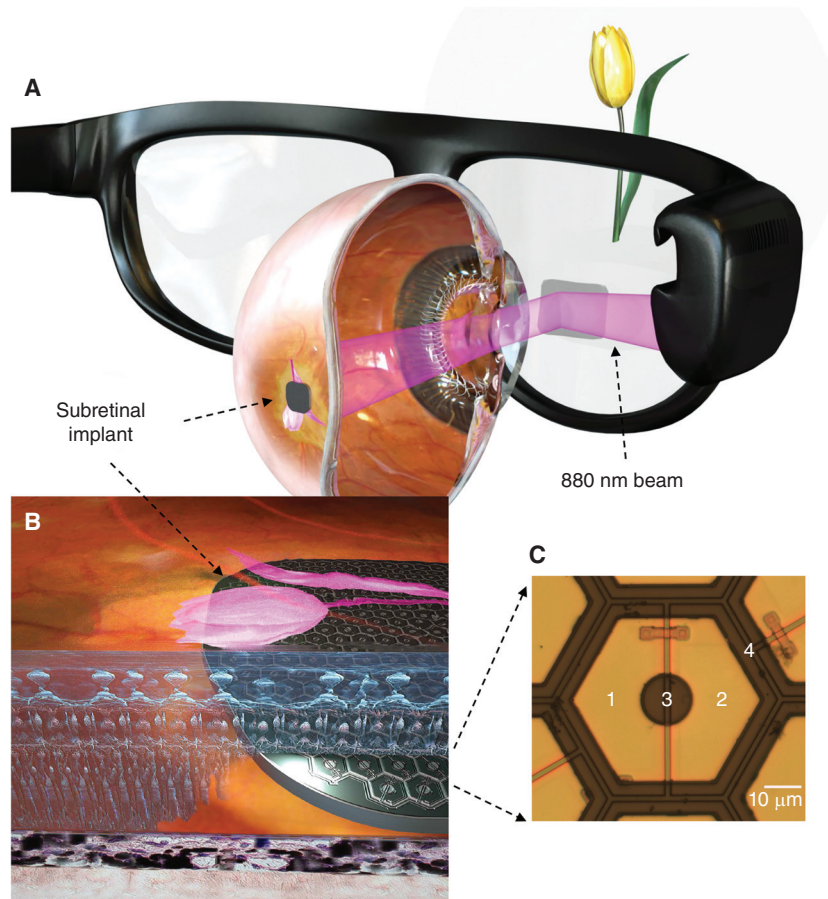


Figure 4. PRIMA: a subretinal photovoltaic implant. (A) Images captured by a camera in the augmented-reality glasses are processed and projected into the eye using pulsed near infrared (880 nm) light. (B) Pixels in the 30- μm -thick subretinal implant convert incident light into electric current flowing through the retina to stimulate the bipolar cells. (C) A 55 μm pixel is composed of two diodes (1 and 2) connected in a series between the active (3) and return (4) electrodes. Scale bar, 10 μm .

(Harnois et al. 1984). This is much smaller than the average size of the RGC receptive fields in rats ($\sim 200 \mu\text{m}$) (Lorach et al. 2015). The difference might be due to nonlinear spatial integration of BC subunits connected to the same ganglion cell RGCs, which allows detecting much finer structures over their receptive fields (Caldwell and Daw 1978; Thibos and Levick 1983; Demb et al. 1999; Brown et al. 2000; Passaglia et al. 2002; Petrusca et al. 2007; Heine and Passaglia 2011; Schwartz et al. 2012). This feature is preserved with subretinal electrical stimulation (Lorach et al. 2015). Spatial resolution measured with alternating gratings projected onto the sub-

retinal photovoltaic pixels of 75 μm and 55 μm in size matched the row pitch of the hexagonal array: 65 μm (Lorach et al. 2015) and 48 μm (Ho et al. 2019), respectively.

Contrast Sensitivity

Similar multiple electrode array (MEA) measurements of the retinal response to steps in irradiance demonstrated the contrast threshold of $\pm 12\%$ with photovoltaic stimulation in the degenerate retinas, as opposed to $\pm 2.3\%$ with visible light in healthy retinas (Ho et al. 2018b). Interestingly, observed decrease of the

D. Palanker

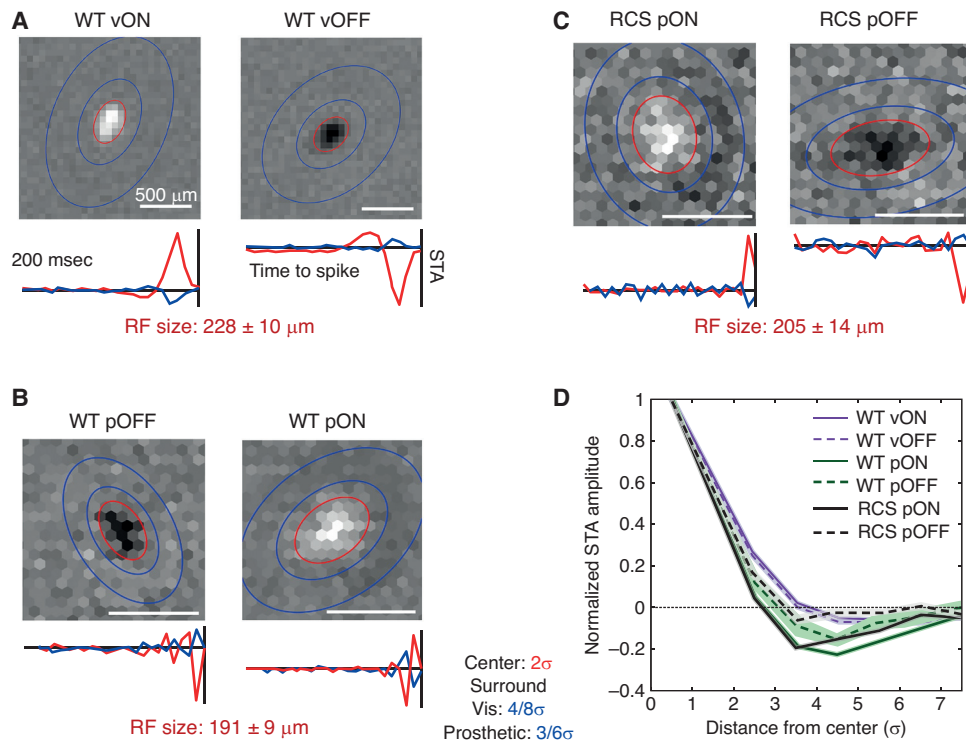


Figure 5. Center-surround organization of the natural and prosthetic receptive fields. (A) The visual spike-triggered average (STA) receptive fields of the ON and OFF retinal ganglion cell (RGC) in the healthy rat retina. The time courses for center and for surround are shown at the *bottom*. (B) Receptive fields and the time courses for photovoltaic response in the healthy rat retina. The vON cells become pOFF, and vOFF cells—pON. (C) Similar receptive field maps and the center and surround time courses for pON and pOFF RGCs in a degenerate rat retina (RCS). (D) The average STA response amplitude, normalized to the deflection in the most central bin versus distance from the center of the receptive field, measured in standard deviations of the 2D Gaussian fit to the STA receptive field. Visual and photovoltaic OFF responses were inverted for ease of comparison.

contrast sensitivity by a factor of 5 in prosthetic vision is similar in magnitude to the natural contrast enhancement between the photoreceptors and BCs (Burkhardt and Fahey 1998), which is absent in the degenerate retina. Loss of this contrast enhancement can be compensated by image processing prior to its delivery to a subretinal implant.

In Vivo Characterization of Prosthetic Vision

Common characteristics of vision, such as resolution, contrast sensitivity, and dynamic range, have been studied extensively with retinal implants (Behrend et al. 2011; Lorach et al. 2015; Ho et al. 2018a,b, 2019). Perception of motion, thought to be transmitted to the brain by the

magnocellular-projecting parasol cells in the primate visual system (Newsome et al. 1985; Merigan and Maunsell 1993), has also been explored with epiretinal implants. Promising results were reported with elicitation of naturalistic motion stimuli in the primate retina (Jepson et al. 2014).

Studies *in vivo* begin with implantation of the devices in an adequate animal model, such as a subretinal photovoltaic prosthesis in rats (Mandel et al. 2013) for example. In this case, surgery begins with a scleral incision, followed by a retinal detachment using injection of saline. The implant is then slid into the gap, which is subsequently sutured. Integration of the device into the subretinal space can be evaluated by retinal imaging, including optical coherence to-

mography (OCT), fundus imaging, and fluorescein angiography.

To characterize prosthetic vision, visually evoked potentials (VEPs), can be measured via transcranial screw electrodes implanted over the visual cortex. Corneal signals can help evaluate the electric current produced by individual pixels (Lorach et al. 2015). Behavioral measurements have also been used in assessment of the stimulation thresholds, contrast sensitivity, ON and OFF responses, and other characteristics of vision (Prevot et al. 2017; Ho et al. 2018b).

Lateral Resolution

Natural and prosthetic visual acuity was studied in rats by recording the VEPs in response to alternating gratings (Fig. 6). This method matches well the visual acuity measured in behavioral tests of natural vision (Dean 1981; Silveira et al. 1987). Grating acuity measured with subretinal photovoltaic pixels of 75 μm (Lorach et al. 2015), 55 μm (Ho et al. 2019), and 40 μm (Wang et al. 2022) in size matched the row pitch of the hexagonal arrays. However, with 20 μm

pixels, prosthetic acuity did not exceed their natural level of 28 μm , indicating that the limiting factor became the retinal signal integration (Wang et al. 2022).

Behavioral tests of subretinal photovoltaic implants PRIMA (Pixium Vision, Paris, France), based on saccadic response to stimulation with 140 μm pixels in nonhuman primates, demonstrated perceptual thresholds of 0.2 mW/mm^2 with 10 msec pulses (Prevot et al. 2017), similar to the earlier observations in RCS rats (Ho et al. 2018b). These measurements also demonstrated visual response with a spot size down to a single pixel.

Contrast Sensitivity

For behavioral measurements of contrast sensitivity, RCS rats with photovoltaic subretinal implants were placed in cages surrounded by near infrared (NIR) displays. Bursts of pulses at various irradiance levels and durations were applied at 20 Hz frequency for 2 sec. Rats' startling response to changes in lighting revealed the average contrast threshold of 12%, as compared to

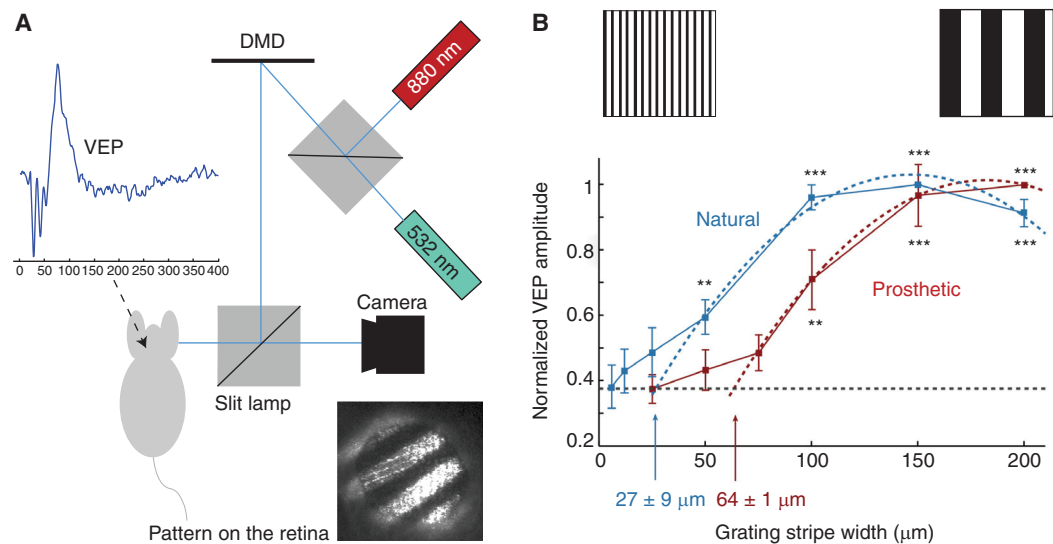


Figure 6. Visual acuity measurements in vivo. (A) Diagram of the setup with visible or near infrared (NIR) laser illumination of a digital micromirror device (DMD) imaged onto the retina. Visual evoked potential (VEP) signals are recorded from three transcranial electrodes. (B) Amplitude of the VEP in response to alternating gratings decreases with the decreasing stripe width, and acuity is defined as an intersection of the extrapolated fit with the noise level.

D. Palanker

2.3% with visible light stimulation in healthy controls (Long–Evans rats) matching the *ex vivo* results described above (Ho et al. 2018b).

Frequency Dependence

Amplitude of the rat VEP in response to pulsatile stimulation decreased with frequency for both the subretinal prosthetic and natural vision in a similar manner: it decreased by half at 10 Hz, compared to 2 Hz, and became practically undetectable at 60 Hz (Ho et al. 2019). Human tests of prosthetic vision with subretinal photovoltaic array, described below, confirmed the flicker fusion between 30 and 60 Hz (Palanker et al. 2020).

CLINICAL EVALUATION

Prosthetic vision in human patients is assessed by a wide variety of psychophysical methods. Several companies and research consortia have reached the clinical phase, thereby providing invaluable evidence that implants can elicit meaningful visual percepts in patients blinded by retinal degenerations. In this section, we review the current status and clinical outcomes with several retinal prostheses.

Criteria for Evaluating Prosthetic Vision

The nonbinding FDA recommendations for assessment of the visual function were issued as a part of their investigational device exemption (IDE) guidance for retinal prostheses (Cohen and Lepri 2013). The suggested tests include the following: (1) low vision letter acuity with limited response time; (2) grating acuity using a forced-choice paradigm and fixed presentation time; (3) mapping of stimulated visual phosphene fields, including two-point discrimination; and (4) assessment of form vision and functional vision in real-world situations, including orientation and mobility. The Second Sight Medical Implants (Sylmar, CA) introduced a set of low vision tests, called FLORA (Functional Low-Vision Observer Rated Assessment), for their Argus II retinal prosthesis trial (Ho et al. 2015). More recently, another set of tests and

measurement methodologies was suggested by a group of investigators working on prosthetic vision (Ayton et al. 2020).

Reports on prosthetic light perception in the other clinical trials describe the perceived brightness, shape, and color of the elicited phosphenes (Ayton et al. 2014; Stingl et al. 2015). In addition to the grating visual acuity, some patients could distinguish Landolt C optotypes and letters. Some reports include temporal characteristics of prosthetic vision and detection of motion.

The Argus II Epiretinal Prosthesis

The only retinal prosthesis approved for commercial use by the FDA (as a humanitarian use device) was the Argus II epiretinal prosthetic system (Second Sight Medical Products, Sylmar, CA). Its head-mounted unit includes a video camera and an RF antenna, which transmits the data and power to the intraocular receiver via serial telemetry (Fig. 2). The signals are then decoded and processed inside the implant, before being distributed via a transscleral cable to the 60 stimulating electrodes on a flexible epiretinal array. Electrodes are 200 μm in diameter, arranged in a square grid with a 575 μm pitch (da Cruz et al. 2016). The array was floating, on average, at 180 μm above the retina (Ahuja et al. 2013). The Argus II has been implanted in more than 200 RP patients, with the best reported grating visual acuity of 20/1260 (Ho et al. 2015). Serious adverse events (SAEs) reported over the course of the clinical trial affected ~30% of the patients, the majority (82%) of which occurred within the first 6 mo. The most common occurrences included conjunctival erosion and dehiscence over the extraocular implant (Ho et al. 2015). No device failures were reported within 3 yr after implantation (Ho et al. 2015).

All patients in the Argus II trial perceived light with the implant turned ON, and almost all subjects performed better at the square localization test with the implant ON than without it. Only 57% of the patients improved in detection of the direction of motion with the system ON versus OFF. Improvements in orientation and mobility with the system was also reported by

the clinical trial, but in other studies, a significantly worse performance at spatial orientation tasks with the implant was observed (Garcia et al. 2014). One reason for this discrepancy could be that prosthetic visual percepts interfered with patient's natural orientation habits, including tactile and auditory perception. Alternatively, Argus II could complicate the spatial orientation since its visual percepts are unrelated to the direction of gaze. Adding the eye tracking with the corresponding shift of the images on the implant indeed improved the object localization (Caspi et al. 2018).

A significant problem with the Argus II epiretinal implant is the stimulation of axons passing near the electrodes from remote RGCs. Percepts induced by axonal stimulation have arcuate rather than punctate shapes (Behrend et al. 2011; Nanduri et al. 2012), which severely distorts a retinotopic map of the visual field. One solution to this problem can be in application of much longer pulses (>25 msec instead of the typical 0.5–1 msec) to activate the BCs rather than ganglion cells, thereby evoking the network-mediated retinal responses without an axonal stimulation (Weitz et al. 2015).

None of the RP patients with Argus II gained vision to the extent that would allow ambulation without a white cane or a guide dog. In March 2019, Second Sight closed the Argus II project, and turned its focus to the cortical visual prosthesis, called Orion (Beauchamp et al. 2020).

The Subretinal Implant Alpha IMS/AMS

The subretinal approach has been spearheaded by the Retina Implant AG (Reutlingen, Germany) with their Alpha IMS system (Zrenner et al. 2011), which received CE mark in 2013. In this device, a subretinal chip with light-sensitive pixels and amplifiers converts images projected naturally by ambient light onto the retina into electrical currents that flow through the retina and stimulate the inner retinal neurons (Fig. 3).

This implant includes 1600 (40×40) pixels of $70 \times 70 \mu\text{m}^2$ in size, each having a photodiode, an amplifier, and a $30 \mu\text{m}$ diameter TiN or SIROF electrode arranged into an array of $2.8 \times 2.8 \text{ mm}$ in size, corresponding to a visual field of

9.3° (Fig. 3). Biphasic pulses (cathodic phase first) ranging from 0.1 to 2.0 msec in duration are applied at frequencies of 0.5–500 Hz to all electrodes. Patients could adjust the photodiode sensitivity and the maximum current according to the ambient lighting conditions and the individual retinal response (Stingl et al. 2017; Daschner et al. 2018). The return electrode, common to all the pixels, is located at the power supply behind the ear. Power is delivered to the implant via a cable that runs under the retina, crossing the sclera pars-plana, and then subdermally to an implant located behind the ear, where power is transmitted via an RF coil (Fig. 3), as in the cochlear implants.

The detection, localization, and counting of objects was significantly better with the implant ON than OFF in 13 out of 15 RP patients in a trial. With foveal placement of the implant ($n = 8$), functional outcomes were significantly better than with parafoveal ($n = 12$): 75% of the patients with foveal location of the chip distinguished a direction of motion, while none of the patients with nonfoveal placement could accomplish this task (Stingl et al. 2013). Two patients could detect Landolt C at 20/546 acuity, which is about half of the Nyquist sampling limit for $70 \mu\text{m}$ pixels (20/280). Twelve patients demonstrated a grating acuity ranging from between 0.1 and 3.3 cpd (Stingl et al. 2017), and 4.6 ± 0.8 gray levels could be distinguished, on average.

The eye movements of RP patients without stimulation were large and scanning. However, with the implant ON, they significantly improved: patients could fixate well and they exhibited the classic fixational movement patterns, such as ocular tremor, drift, and microsaccades (Hafed et al. 2016).

The majority of the Alpha IMS implants failed within a year postimplantation, while half of the Alpha AMS devices failed within 30 mo (Daschner et al. 2018). In March 2019, Retina Implant AG closed.

A Photovoltaic Subretinal Implant PRIMA

The photovoltaic PRIMA implant (Pixium Vision, Paris) is designed for restoration of central vision in patients impaired by GA in AMD.

D. Palanker

Photodiodes in each pixel convert light into biphasic (anodic first) pulses of electric current (Lorach et al. 2015). The implant used in the first feasibility trial was 2×2 mm in width (corresponding to about 7° of the visual field), 30 μm thick, with 378 pixels of 100 μm in size (Palanker et al. 2020). Images captured by the camera are processed and projected from the augmented-reality (AR) glasses into an 18° wide field on the retina. To avoid photophobic and phototoxic effects of bright illumination, NIR (880 nm) light is applied (Fig. 4; Goetz et al. 2013). For a steady perception under pulsed illumination, frequencies exceeding the flicker fusion are applied (30–60 Hz). Perceptual brightness is adjusted by modulating the pulse duration in a DMD display of the AR glasses from 0.7 to 10 msec.

The first feasibility study was conducted in five patients with GA of at least three optic disc diameters and a visual acuity 20/400–20/1000 in the worse-seeing “study” eye. Residual natural acuity due to preserved peripheral vision and eccentric fixation did not decrease after the implantation in any of the patients, demonstrating the safety and stability of the submacular chip, with a follow-up period now exceeding 36 mo. Prosthetic vision was initially tested using the virtual-reality glasses (PRIMA-1), and then with augmented-reality glasses (PRIMA-2).

All five patients perceived monochromatic (white-yellowish “sun color”) patterns with the brightness adjustable by pulse duration in the range of 0.7–10 msec in retinotopically correct locations within the previous scotomata. All four patients with a subretinal placement of the chip demonstrated Landolt C acuity of 1.17 ± 0.13 pixels, corresponding to the Snellen range of 20/438–20/564 (Palanker et al. 2020, 2022). Such a close match of prosthetic acuity to the pixel size indicates that smaller pixels may provide even higher resolution and hence offer real benefits to a larger number of patients. Remarkably, patients perceive simultaneously the prosthetic central vision and peripheral natural vision in the treated and in the fellow eye (Palanker et al. 2022).

Interestingly, despite the lack of selectivity in stimulation of the ON and OFF BCs, patients perceive the displayed images in a correct con-

trast: for example, as light patterns on a dark background, and not as a mixture of the bright and dark spots. One reason could be that the rod BCs have only the ON pathway, split into ON and OFF RGCs via amacrine cells, so there should be no polarity reversal upon electrical stimulation here. Similarly, the ON-cone pathway should preserve the polarity of the RGC response under electrical stimulation. The OFF-cone pathway is expected to be reversed in electrical stimulation, but its input into the visual system may be attenuated by the low signal-to-noise ratio since spontaneous firing in OFF-RGCs greatly increases in retinal degeneration (Sekirnjak et al. 2011; Denlinger et al. 2020). Another potential difference is the fact that ON BCs have longer axons than the OFF BCs (Euler et al. 2014) and therefore should experience a larger voltage step across the cell in a similar electric field, yielding a stronger response than the OFF BCs.

A noticeable difference between the prosthetic and natural vision is a slower than normal image recognition, even when resolution is not a limiting factor. This might be due to a lower number of BCs activated electrically than naturally due to the limited penetration depth of electric field into the INL. Reduced flow of the visual information may be compensated by longer integration (Ho et al. 2020).

Suprachoroidal Systems

A suprachoroidal placement of the electrode array has been tested by Bionic Vision Australia (three patients) (Ayton et al. 2014) and by a group in Osaka University (two patients) (Fujikado et al. 2011). Phosphene perception in RP patients was reported over the 12-month Bionic Vision trial, but the equivalent visual acuity was in the realm of ultralow vision, ranging from 20/4000 to 20/20,000. Its utility for ambulation and object localization remains to be explored (Kolic et al. 2020).

Other Clinical Results

Optobionics Inc. conducted a clinical trial of their subretinal array of photodiodes (artificial silicon retina [ASR]). They reported improve-



ments in central vision following implantation of the ASR in the periphery, possibly due to neurotrophic effects of surgery or of the implant (Chow et al. 2004). The company closed in 2007. The EPIRET3—an epiretinal array of 25 electrodes of 100 μm in diameter spaced 500 μm apart (Klauke et al. 2011), implanted in six patients for a period of 4 wk, successfully elicited visual percepts. However, the studies did not continue beyond 2010. Clinical trials of the IRIS II epiretinal implant with 150 electrodes have been conducted by Pixium Vision (Muqit et al. 2019). Patients reported some visual percepts, but the trial was discontinued in 2017.

In early 2020, Nano Retina started a clinical trial of their NR600 epiretinal implant in patients with advanced RP. Wireless implant includes a camera, image processor, and an array of 600 electrodes spaced by 100 μm and penetrating by about 100 μm into the retina. Implant is powered by NIR light emitted from the glasses (Nano Retina [Yanovitch et al. 2022]). First reports of the clinical outcomes include localization of a square of light on a screen, and the ability to follow a white line on the floor.

SUMMARY AND OUTLOOK

The first two companies that tested an idea of electronic restoration of sight in patients blinded by inherited retinal degeneration (RP) using epiretinal (Second Sight) and subretinal (Retina Implant AG) implants have proven the concept. However, since they failed to reach satisfactory performance, both products were discontinued in 2019, after about 20 yr of development. Commercialization of such a complex technology for a relatively small market is one of the challenges, and therefore such projects are usually undertaken by consortiums of academic research groups and commercial companies. The next generation of implants and stimulation protocols is designed to address some of the shortcomings of the first systems.

On a subretinal side, the wireless nature of the photovoltaic implant PRIMA enables its application to AMD patients, where retinal network is better preserved than in the end-stage RP. In addition, local return electrodes in PRIMA pixels

provide much better confinement of electric field than with a remote return, thereby improving contrast, selectivity, and resolution of retinal stimulation (Palanker et al. 2022). The next challenge is to reduce the pixel size down to 25 μm and achieve acuity of 20/100, which would provide real benefit to many AMD patients. Iridium Medical Technology (www.irmedtech.com/Advantage/index_en.html) is developing a flexible retinal implant to cover a wide visual field, essential for ambulation of RP patients.

On the epiretinal side, an implant for selective activation of the many classes of RGCs with the appropriate retinal code is being developed for the end-stage RP patients (Shah and Chichilnisky 2020). A group of D. Ghezzy at EPFL is developing a flexible epiretinal implant to cover a wide visual field, essential for ambulation of RP patients (Woodburn et al. 2002; Chenais et al. 2021), as described below.

Electric Field Shaping for High Resolution in Subretinal Approach

Distance between the implant and the target neurons becomes a limiting factor when it exceeds the electrode size or a separation between the active and return electrodes (Fig. 7A; Palanker et al. 2005; Loudin et al. 2007; Flores et al. 2019). Since the INL thickness is $\sim 30\text{--}40$ μm , planar bipolar implants with local return electrodes and pixel pitch smaller than 60 μm (30 μm radius) are unlikely to stimulate all the neurons in the INL within the safe charge injection limits (Flores et al. 2019).

One way to improve the proximity to the target neurons is to use three-dimensional electrodes, such as pillars and honeycombs, using retinal migration into the voids (Fig. 7B,C). Recent measurements with 40 and 55 μm pixels in rats demonstrated that 10 μm tall pillar electrodes reduce the stimulation threshold by half (Ho et al. 2019). Honeycombs are expected to provide even bigger benefit since the insulating walls between the pixels direct the electric field vertically, along the BCs in the retina, and thereby decreasing the stimulation threshold (Flores et al. 2019). These walls also decouple the field penetration depth from the pixel width, making

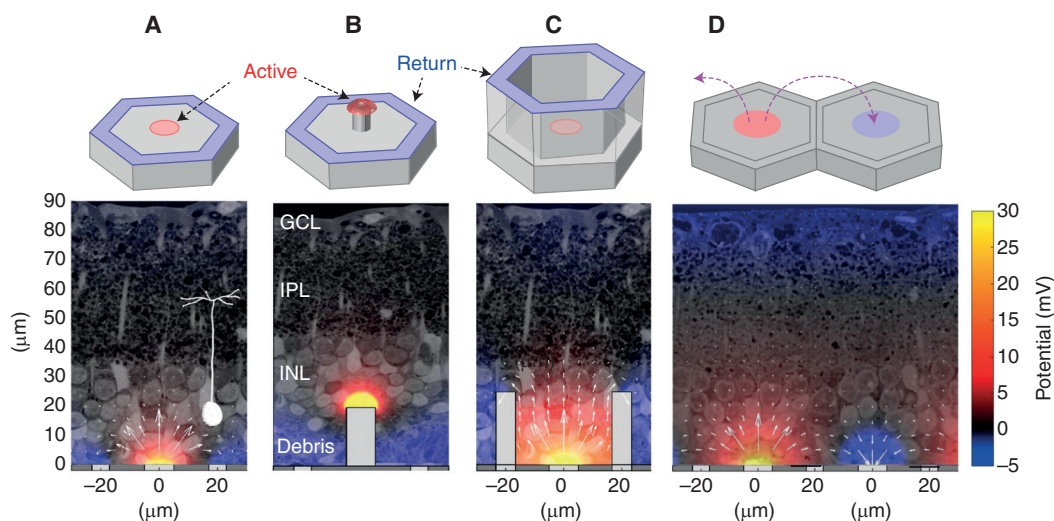


Figure 7. Electric field shaping strategies. (A) As flat bipolar pixels decrease in size, penetration of electric field into the retina becomes insufficient for stimulation of the bipolar cells (diagrammatically shown in white on top of the retinal histology). (B,C) Within a few weeks postimplantation, cells in the inner nuclear layer (INL) migrate into the voids between the pillars or walls in the subretinal implant, thereby getting closer to the active electrodes. (C) With a return electrode on top of the walls, an electric field is aligned vertically, along the bipolar cells. Since the field penetration depth is decoupled from the pixel width, stimulation threshold does not change with the pixel size. (D) Current steering, with some pixels serving as anodes and some as cathodes intermittently, enables field shaping for optimal lateral and axial confinement. (GCL) Ganglion cell layer, (IPL) inner plexiform layer.

the stimulation threshold independent of pixel width.

Yet another possibility for the optimal field confinement is a current steering, where active electrodes can be used as anodes and as cathodes intermittently (Fig. 7D). Such a strategy may allow optimizing the electric field penetration depth and lateral confinement for every patient, depending on the retinal thickness and its proximity to the implant (Wang et al. 2022).

Selective Stimulation of RGCs

A group called “Artificial Retina,” led by Dr. Chichilnisky at Stanford, is working on a device for selective activation of RGCs to mimic the natural retinal code for proper restoration of sight (Shah and Chichilnisky 2020). During the initial calibration, the epiretinal implant will record and identify the many distinct RGC types based on characteristics of their spontaneous firing. The implant will then activate the appropriate ganglion cells at the appropriate times, effectively trans-

forming the captured visual scene into the proper spiking sequence of the various cells.

Flexible Implants for a Wide Visual Field

For a comfortable ambulation of the patients blinded by RP, the prosthetic visual field should exceed 20°, which corresponds to 6 mm length on the retina. To ensure proximity to the retina over such a large area, implants should follow the eye curvature. Two groups are working on wide flexible implants to address this need: an epiretinal array based on organic photodiodes (Polyretina) (Chenais et al. 2021), and a subretinal device based on flexible CMOS electronics (Iridium Medical) (Woodburn et al. 2002).

Image Processing

In addition to improvements in esthetic appearance and in optical performance of the virtual and augmented reality glasses, prosthetic vision may advance with applications of advanced im-

age processing. Besides the obvious functions, such as optical or electronic zoom, contrast enhancement, and autofocus of the camera, visual scenes could be simplified prior to projection onto the implant, which would help better match its resolution and contrast and make the visual percepts easier to understand. Computer algorithms rapidly advance at visual categorization (e.g., segregation of the visual content by distance and displaying only the closer objects [Jung et al. 2015]) or by encoding the depth instead of luminance to facilitate navigation (Hicks et al. 2014) have been recently demonstrated. Other improvements may include simplified or symbolic representation of common objects, such as banknotes, as well as integration of the other assistive technologies, such as text-to-voice conversion, face recognition, etc.

REFERENCES

- Ahuja AK, Dorn JD, Caspi A, McMahon MJ, Dagnelie G, Dacruz L, Stanga P, Humayun MS, Greenberg RJ. 2011. Blind subjects implanted with the Argus II retinal prosthesis are able to improve performance in a spatial-motor task. *Br J Ophthalmol* **95**: 539–543. doi:10.1136/bjo.2010.179622
- Ahuja AK, Yeoh J, Dorn JD, Caspi A, Wuyyuru V, McMahon MJ, Humayun MS, Greenberg RJ, Dacruz L. 2013. Factors affecting perceptual threshold in Argus II retinal prosthesis subjects. *Transl Vis Sci Technol* **2**: 1. doi:10.1167/tvst.2.4.1
- Ayton LN, Blamey PJ, Guymer RH, Luu CD, Nayagam DA, Sinclair NC, Shivdasani MN, Yeoh J, McCombe MF, Briggs RJ, et al. 2014. First-in-human trial of a novel suprachoroidal retinal prosthesis. *PLoS ONE* **9**: e115239. doi:10.1371/journal.pone.0115239
- Ayton LN, Rizzo JF, Bailey IL, Colenbrander A, Dagnelie G, Geruschat DR, Hessburg PC, McCarthy CD, Petoe MA, Rubin GS, et al. 2020. Harmonization of outcomes and vision endpoints in vision restoration trials: recommendations from the International HOVER Taskforce. *Transl Vis Sci Technol* **9**: 25. doi:10.1167/tvst.9.8.25
- Beauchamp MS, Oswald D, Sun P, Foster BL, Magnotti JF, Niketeghad S, Pouratian N, Bosking WH, Yoshor D. 2020. Dynamic stimulation of visual cortex produces form vision in sighted and blind humans. *Cell* **181**: 774–783.e5. doi:10.1016/j.cell.2020.04.033
- Behrend MR, Ahuja AK, Humayun MS, Chow RH, Weiland JD. 2011. Resolution of the epiretinal prosthesis is not limited by electrode size. *IEEE Trans Neural Syst Rehabil Eng* **19**: 436–442. doi:10.1109/TNSRE.2011.2140132
- Boinagrov D, Loudin J, Palanker D. 2010. Strength-duration relationship for extracellular neural stimulation: numerical and analytical models. *J Neurophysiol* **104**: 2236–2248. doi:10.1152/jn.00343.2010
- Boinagrov D, Pangratz-Fuehrer S, Goetz G, Palanker D. 2014. Selectivity of direct and network-mediated stimulation of the retinal ganglion cells with epi-, sub- and intraretinal electrodes. *J Neural Eng* **11**: 026008. doi:10.1088/1741-2560/11/2/026008
- Brown SP, He S, Masland RH. 2000. Receptive field microstructure and dendritic geometry of retinal ganglion cells. *Neuron* **27**: 371–383. doi:10.1016/S0896-6273(00)00044-1
- Burkhardt DA, Fahey PK. 1998. Contrast enhancement and distributed encoding by bipolar cells in the retina. *J Neurophysiol* **80**: 1070–1081. doi:10.1152/jn.1998.80.3.1070
- Cai C, Ren Q, Desai NJ, Rizzo JF III, Fried SI. 2011. Response variability to high rates of electric stimulation in retinal ganglion cells. *J Neurophysiol* **106**: 153–162. doi:10.1152/jn.00956.2010
- Caldwell JH, Daw NW. 1978. New properties of rabbit retinal ganglion cells. *J Physiol* **276**: 257–276. doi:10.1113/jphysiol.1978.sp012232
- Caspi A, Roy A, Wuyyuru V, Rosendall PE, Harper JW, Katyal KD, Barry MP, Dagnelie G, Greenberg RJ. 2018. Eye movement control in the Argus II retinal-prosthesis enables reduced head movement and better localization precision. *Invest Ophthalmol Vis Sci* **59**: 792–802. doi:10.1167/iovs.17-22377
- Chen ZC, Wang BY, Palanker D. 2020. Real-time optimization of the current steering for visual prosthesis. In *Proceedings of the 10th International IEEE/EMBS Conference on Neural Engineering (NER)*. Virtual Event, May 4–6.
- Chenais NAL, Leccardi MJIA, Ghezzi D. 2021. Photovoltaic retinal prosthesis restores high-resolution responses to single-pixel stimulation in blind retinas. *Commun Mater* **2**: 28. doi:10.1038/s43246-021-00133-2
- Chichilnisky EJ, Kalmar RS. 2002. Functional asymmetries in ON and OFF ganglion cells of primate retina. *J Neurosci* **22**: 2737–2747. doi:10.1523/JNEUROSCI.22-07-02737.2002
- Cho A, Ratliff C, Sampath A, Weiland J. 2016. Changes in ganglion cell physiology during retinal degeneration influence excitability by prosthetic electrodes. *J Neural Eng* **13**: 025001. doi:10.1088/1741-2560/13/2/025001
- Chow AY, Chow VY, Packo KH, Pollack JS, Peyman GA, Schuchard R. 2004. The artificial silicon retina microchip for the treatment of vision loss from retinitis pigmentosa. *Arch Ophthalmol-Chic* **122**: 460–469. doi:10.1001/archopht.122.4.460
- Cohen E, Lepri B. 2013. Investigational device exemption guidance for retinal prostheses. In *The senses: a comprehensive reference*, 2nd ed. Center for Devices and Radiological Health-FDA, Elsevier, Amsterdam.
- da Cruz L, Coley BF, Dorn J, Merlini F, Filley E, Christopher P, Chen FK, Wuyyuru V, Sahel J, Stanga P, et al. 2013. The Argus II epiretinal prosthesis system allows letter and word reading and long-term function in patients with profound vision loss. *Br J Ophthalmol* **97**: 632–636. doi:10.1136/bjophthalmol-2012-301525
- da Cruz L, Dorn JD, Humayun MS, Dagnelie G, Handa J, Barale PO, Sahel JA, Stanga PE, Hafezi F, Safran AB, et al. 2016. Five-year safety and performance results from the Argus II retinal prosthesis system clinical trial. *Ophthalmology* **123**: 2248–2254. doi:10.1016/j.ophtha.2016.06.049

D. Palanker

- Daschner R, Greppmaier U, Kokelmann M, Rudolf S, Rudolf R, Schleeauf S, Wrobel WG. 2017. Laboratory and clinical reliability of conformally coated subretinal implants. *Biomed Microdevices* **19**: 7. doi:10.1007/s10544-017-0147-6
- Daschner R, Rothermel A, Rudolf R, Rudolf S, Stett A. 2018. Functionality and performance of the subretinal implant chip Alpha AMS. *Sensor Mater* **30**: 179–192. doi:10.18494/SAM.2018.1726
- Dean P. 1981. Visual pathways and acuity hooded rats. *Behav Brain Res* **3**: 239–271. doi:10.1016/0166-4328(81)90050-4
- Demb JB, Haarsma L, Freed MA, Sterling P. 1999. Functional circuitry of the retinal ganglion cell's nonlinear receptive field. *J Neurosci* **19**: 9756–9767. doi:10.1523/JNEUROSCI.19-22-09756.1999
- Denlinger B, Helft Z, Telias M, Lorach H, Palanker D, Kramer RH. 2020. Local photoreceptor degeneration causes local pathophysiological remodeling of retinal neurons. *JCI Insight* **5**: e132114. doi:10.1172/jci.insight.132114
- Euler T, Haverkamp S, Schubert T, Baden T. 2014. Retinal bipolar cells: elementary building blocks of vision. *Nat Rev Neurosci* **15**: 507–519. doi:10.1038/nrn3783
- Field GD, Sher A, Gauthier JL, Greschner M, Shlens J, Litke AM, Chichilnisky EJ. 2007. Spatial properties and functional organization of small bistratified ganglion cells in primate retina. *J Neurosci* **27**: 13261–13272.
- Flores T, Goetz G, Lei X, Palanker D. 2016. Optimization of return electrodes in neurostimulating arrays. *J Neural Eng* **13**: 036010. doi:10.1088/1741-2560/13/3/036010
- Flores T, Huang T, Bhuckory M, Ho E, Chen Z, Dalal R, Galambos L, Kamins T, Mathieson K, Palanker D. 2019. Honeycomb-shaped electro-neural interface enables cellular-scale pixels in subretinal prosthesis. *Sci Rep* **9**: 10657. doi:10.1038/s41598-019-47082-y
- Fried SI, Hsueh HA, Werblin FS. 2006. A method for generating precise temporal patterns of retinal spiking using prosthetic stimulation. *J Neurophysiol* **95**: 970–978. doi:10.1152/jn.00849.2005
- Fried SI, Lasker ACW, Desai NJ, Eddington DK, Rizzo JF. 2009. Axonal sodium-channel bands shape the response to electric stimulation in retinal ganglion cells. *J Neurophysiol* **101**: 1972–1987.
- Friedman DS, O'Colmain BJ, Munoz B, Tomany SC, McCarty C, de Jong PT, Nemesure B, Mitchell P, Kempen J; Eye Diseases Prevalence Research Group. 2004. Prevalence of age-related macular degeneration in the United States. *Arch Ophthalmol* **122**: 564–572.
- Fujikado T, Kamei M, Sakaguchi H, Kanda H, Morimoto T, Ikuno Y, Nishida K, Kishima H, Maruo T, Konoma K. 2011. Testing of semichronically implanted retinal prosthesis by suprachoroidal-transretinal stimulation in patients with retinitis pigmentosa. *Invest Ophthalmol Vis Sci* **52**: 4726–4733. doi:10.1167/iovs.10-6836
- Garcia S, Petrini K, Da Cruz L, Rubin GS, Nardini M. 2014. Assessing improvements in perception afforded by retinal prostheses in multisensory tasks. *Invest Ophthalmol Vis Sci* **55**: 5962.
- Ghezzi D, Antognazza MR, Maccarone R, Bellani S, Lanzarini E, Martino N, Mete M, Pertile G, Bisti S, Lanzani G, et al. 2013. A polymer optoelectronic interface restores light sensitivity in blind rat retinas. *Nat Photonics* **7**: 400–406. doi:10.1038/nphoton.2013.34
- Goetz GA, Mandel Y, Manivanh R, Palanker DV, Čížmár T. 2013. Holographic display system for restoration of sight to the blind. *J Neural Eng* **10**: 056021. doi:10.1088/1741-2560/10/5/056021
- Grosberg LE, Ganesan K, Goetz GA, Madugula SS, Bhaskar N, Fan V, Li P, Hottowy P, Dabrowski W, Sher A, et al. 2017. Activation of ganglion cells and axon bundles using epiretinal electrical stimulation. *J Neurophysiol* **118**: 1457–1471. doi:10.1152/jn.00750.2016
- Ha S, Khraiche ML, Akinin A, Jing Y, Damle S, Kuang Y, Bauchner S, Lo YH, Freeman WR, Silva GA, et al. 2016. Towards high-resolution retinal prostheses with direct optical addressing and inductive telemetry. *J Neural Eng* **13**: 056008. doi:10.1088/1741-2560/13/5/056008
- Hafed ZM, Stingl K, Bartz-Schmidt KU, Gekeler F, Zrenner E. 2016. Oculomotor behavior of blind patients seeing with a subretinal visual implant. *Vision Res* **118**: 119–131.
- Haim M. 2022. Epidemiology of retinitis pigmentosa in Denmark. *Acta Ophthalmol Scand Suppl* **233**: 1–34.
- Harnois C, Bodis-Wollner I, Onofrij M. 1984. The effect of contrast and spatial frequency on the visual evoked potential of the hooded rat. *Exp Brain Res* **57**: 1–8.
- Heine WF, Passaglia CL. 2011. Spatial receptive field properties of rat retinal ganglion cells. *Vis Neurosci* **28**: 403–417. doi:10.1017/S0952523811000307
- Hicks SL, Wilson I, van Rheede JJ, MacLaren RE, Downes SM, Kennard C. 2014. Improved mobility with depth-based residual vision glasses. *Invest Ophthalmol Vis Sci* **55**: 2153.
- Ho AC, Humayun MS, Dorn JD, da Cruz L, Dagnelie G, Handa J, Barale PO, Sahel JA, Stanga PE, Hafezi F, et al. 2015. Long-term results from an epiretinal prosthesis to restore sight to the blind. *Ophthalmology* **122**: 1547–1554.
- Ho E, Smith R, Goetz G, Lei X, Galambos L, Kamins TI, Harris J, Mathieson K, Palanker D, Sher A. 2018a. Spatiotemporal characteristics of retinal response to network-mediated photovoltaic stimulation. *J Neurophysiol* **119**: 389–400. doi:10.1152/jn.00872.2016
- Ho E, Lorach H, Goetz G, Laszlo F, Lei X, Kamins T, Mariani JC, Sher A, Palanker D. 2018b. Temporal structure in spiking patterns of ganglion cells defines perceptual thresholds in rodents with subretinal prosthesis. *Sci Rep* **8**: 3145. doi:10.1038/s41598-018-21447-1
- Ho E, Lei X, Flores T, Lorach H, Huang T, Galambos L, Kamins T, Harris J, Mathieson K, Palanker D. 2019. Characteristics of prosthetic vision in rats with subretinal flat and pillar electrode arrays. *J Neural Eng* **16**: 066027. doi:10.1088/1741-2552/ab34b3
- Ho E, Shmakov A, Palanker D. 2020. Decoding network-mediated retinal response to electrical stimulation: implications for fidelity of prosthetic vision. *J Neural Eng* **17**: 1–24.
- Hornig R, Dapper M, Le Joliff E, Hill R, Ishaque K, Posch C, Benosman R, LeMer Y, Sahel J-A, Picaud S. 2017. Pixium vision: first clinical results and innovative developments. In *Artificial vision: a clinical guide* (ed. Gabel VP), pp. 99–113. Springer, Amsterdam.
- Humayun MS, Prince M, de Juan E, Barron Y, Moskowitz M, Klock IB, Milam AH. 1999. Morphometric analysis of the



- extramacular retina from postmortem eyes with retinitis pigmentosa. *Invest Ophthalmol Vis Sci* **40**: 143–148.
- Humayun MS, Dorn JD, da Cruz L, Dagnelie G, Sahel JA, Stanga PE, Cideciyan AV, Duncan JL, Elliott D, Filley E, et al. 2012. Interim results from the international trial of second sight's visual prosthesis. *Ophthalmology* **119**: 779–788. doi:10.1016/j.ophtha.2011.09.028
- Jensen RJ, Rizzo JF III. 2006. Thresholds for activation of rabbit retinal ganglion cells with a subretinal electrode. *Exp Eye Res* **83**: 367–373. doi:10.1016/j.exer.2006.01.012
- Jensen RJ, Ziv OR, Rizzo JF III. 2005. Thresholds for activation of rabbit retinal ganglion cells with relatively large, extracellular microelectrodes. *Invest Ophthalmol Vis Sci* **46**: 1486–1496. doi:10.1167/iovs.04-1018
- Jepson LH, Hottowy P, Weiner GA, Dabrowski W, Litke AM, Chichilnisky EJ. 2014. High-fidelity reproduction of spatiotemporal visual signals for retinal prosthesis. *Neuron* **83**: 87–92. doi:10.1016/j.neuron.2014.04.044
- Jones BW, Marc RE. 2005. Retinal remodeling during retinal degeneration. *Exp Eye Res* **81**: 123–137. doi:10.1016/j.exer.2005.03.006
- Jung JH, Aloni D, Yitzhaky Y, Peli E. 2015. Active confocal imaging for visual prostheses. *Vision Res* **111** (Part B): 182–196.
- Kim SY, Sada S, Pearlman J, Humayun MS, de Juan E Jr, Melia BM, Green WR. 2002. Morphometric analysis of the macula in eyes with disciform age-related macular degeneration. *Retina* **22**: 471–477. doi:10.1097/00006982-200208000-00012
- Klauke S, Goertz M, Rein S, Hoehl D, Thomas U, Eckhorn R, Bremmer F, Wachtler T. 2011. Stimulation with a wireless intraocular epiretinal implant elicits visual percepts in blind humans. *Invest Ophthalmol Vis Sci* **52**: 449–455.
- Knutson JS, Naples GG, Peckham PH, Keith MW. 2002. Electrode fracture rates and occurrences of infection and granuloma associated with percutaneous intramuscular electrodes in upper-limb functional electrical stimulation applications. *J Rehab Res Devel* **39**: 671–683.
- Kolic M, Baglin EK, Titchener S, Kvasakul J, Abbott CJ, Barnes N, McGuinness M, Kentler W, Young K, Walker J, et al. 2020. A 44 channel suprachoroidal retinal prosthesis: interim functional vision results. *Invest Ophthalmol Vis Sci* **61**: 2199.
- Lee DY, Lorach H, Huie P, Palanker D. 2016. Implantation of modular photovoltaic subretinal prosthesis. *Ophthalmic Surg Lasers Imaging Retina* **47**: 171–174.
- Lorach H, Goetz G, Smith R, Lei X, Mandel Y, Kamins T, Mathieson K, Huie P, Harris J, Sher A, et al. 2015. Photovoltaic restoration of sight with high visual acuity. *Nat Med* **21**: 476–482. doi:10.1038/nm.3851
- Loudin JD, Simanovskii DM, Vijayraghavan K, Sramek CK, Butterwick AF, Huie P, McLean GY, Palanker DV. 2007. Optoelectronic retinal prosthesis: system design and performance. *J Neural Eng* **4**: S72–S84. doi:10.1088/1741-2560/4/1/S09
- Malmivuo J, Plonsey R. 1995. Functional electric stimulation. In *Bioelectromagnetism* (pp. 363–375). Oxford University Press, New York.
- Mandel Y, Goetz G, Lavinsky D, Huie P, Mathieson K, Wang L, Kamins T, Galambos L, Manivanh R, Harris J, et al. 2013. Cortical responses elicited by photovoltaic subretinal prostheses exhibit similarities to visually evoked potentials. *Nat Commun* **4**: 1980.
- Marc RE, Jones BW. 2003. Retinal remodeling in inherited photoreceptor degenerations. *Mol Neurobiol* **28**: 139–147. doi:10.1385/MN:28:2:139
- Marc RE, Jones BW, Watt CB, Strettoi E. 2003. Neural remodeling in retinal degeneration. *Prog Retin Eye Res* **22**: 607–655. doi:10.1016/S1350-9462(03)00039-9
- Margolis DJ, Newkirk G, Euler T, Detwiler PB. 2008. Functional stability of retinal ganglion cells after degeneration-induced changes in synaptic input. *J Neurosci* **28**: 6526–6536. doi:10.1523/JNEUROSCI.1533-08.2008
- Masland RH. 2001. The fundamental plan of the retina. *Nat Neurosci* **4**: 877–886. doi:10.1038/nn0901-877
- Mathieson K, Loudin J, Goetz G, Huie P, Wang L, Kamins TI, Galambos L, Smith R, Harris JS, Sher A, et al. 2012. Photovoltaic retinal prosthesis with high pixel density. *Nat Photon* **6**: 391–397. doi:10.1038/nphoton.2012.104
- Mazzoni F, Novelli E, Strettoi E. 2008. Retinal ganglion cells survive and maintain normal dendritic morphology in a mouse model of inherited photoreceptor degeneration. *J Neurosci* **28**: 14282–14292. doi:10.1523/JNEUROSCI.4968-08.2008
- Menzler J, Zeck G. 2011. Network oscillations in rod-degenerated mouse retinas. *J Neurosci* **31**: 2280–2291. doi:10.1523/JNEUROSCI.4238-10.2011
- Merigan WH, Maunsell JH. 1993. How parallel are the primate visual pathways? *Annu Rev Neurosci* **16**: 369–402. doi:10.1146/annurev.ne.16.030193.002101
- Muqit MMK, Velikay-Parel M, Weber M, Dupeyron G, Audemard D, Corcostegui B, Sahel J, Le Mer Y. 2019. Six-month safety and efficacy of the intelligent retinal implant system II device in retinitis pigmentosa. *Ophthalmology* **126**: 637–639.
- Nanduri D, Fine I, Horsager A, Boynton GM, Humayun MS, Greenberg RJ, Weiland JD. 2012. Frequency and amplitude modulation have different effects on the percepts elicited by retinal stimulation. *Invest Ophthalmol Vis Sci* **53**: 205–214. doi:10.1167/iovs.11-8401
- Naumann J. 2012. *Search for paradise: a patient's account of the artificial vision experiment*. Xlibris, Bloomington, IN.
- Newsome WT, Wurtz RH, Dursteler MR, Mikami A. 1985. Deficits in visual-motion processing following ibotenic acid lesions of the middle temporal visual area of the Macaque monkey. *J Neurosci* **5**: 825–840. doi:10.1523/JNEUROSCI.05-03-00825.1985
- Olveczky BP, Baccus SA, Meister M. 2003. Segregation of object and background motion in the retina. *Nature* **423**: 401–408.
- Palanker D, Blumenkranz MS, Weiter JJ. 2005. Retinal laser therapy: biophysical basis and applications. In *Retina*, Vol 1, 4th ed. (ed. Ryan SJ), pp. 539–553. Mosby, St Louis.
- Palanker D, Le Mer Y, Mohand-Said S, Muqit M, Sahel JA. 2020. Photovoltaic restoration of central vision in atrophic age-related macular degeneration. *Ophthalmology* **127**: 1097–1104. doi:10.1016/j.ophtha.2020.02.024
- Palanker D, Le Mer Y, Mohand-Said S, Sahel JA. 2022. Simultaneous perception of prosthetic and natural vision in AMD patients. *Nat Commun* **13**: 513.

D. Palanker

- Passaglia CL, Troy JB, Rüttiger L, Lee BB. 2002. Orientation sensitivity of ganglion cells in primate retina. *Vision Res* **42**: 683–694. doi:10.1016/S0042-6989(01)00312-1
- Petrusca D, Grivich MI, Sher A, Field GD, Gauthier JL, Greschner M, Shlens J, Chichilnisky EJ, Litke AM. 2007. Identification and characterization of a Y-like primate retinal ganglion cell type. *J Neurosci* **27**: 11019–11027. doi:10.1523/JNEUROSCI.2836-07.2007
- Prevot PH, Lanoë M, Dalouz S, Blaize K, Oubari O, Gehe K, Akolkar H, Buc G, Picaud SA, Sahel JA. 2017. Behavioral and electrophysiological characterization of photovoltaic subretinal implants in non-human primates. *Invest Ophthalmol Vis Sci* **58**: 4270–4270.
- Richard E, Goetz G, Chichilnisky EJ. 2015. Recognizing retinal ganglion cells in the dark. *Adv Neural Inf Proc Syst* **28**: 1–9.
- Rizzo JF 3rd, Shire DB, Kelly SK, Troyk P, Gingerich M, McKee B, Priplata A, Chen J, Drohan W, Doyle P, et al. 2011. Overview of the Boston retinal prosthesis: challenges and opportunities to restore useful vision to the blind. In *Conference proceedings: Annual International Conference of the IEEE Engineering in Medicine and Biology Society IEEE Engineering in Medicine and Biology Society Conference 2011*, pp. 7492–7495.
- Schwartz GW, Okawa H, Dunn FA, Morgan JL, Kerschensteiner D, Wong RO, Rieke F. 2012. The spatial structure of a nonlinear receptive field. *Nat Neurosci* **15**: 1572–1580. doi:10.1038/nn.3225
- Sekirnjak C, Hottowy P, Sher A, Dabrowski W, Litke AM, Chichilnisky EJ. 2006. Electrical stimulation of mammalian retinal ganglion cells with multielectrode arrays. *J Neurophysiol* **95**: 3311–3327. doi:10.1152/jn.01168.2005
- Sekirnjak C, Jepson LH, Hottowy P, Sher A, Dabrowski W, Litke AM, Chichilnisky EJ. 2011. Changes in physiological properties of rat ganglion cells during retinal degeneration. *J Neurophysiol* **105**: 2560–2571. doi:10.1152/jn.01061.2010
- Shah NP, Chichilnisky EJ. 2020. Computational challenges and opportunities for a bi-directional artificial retina. *J Neural Eng* **17**: 055002.
- Shah NP, Madugula S, Grosberg L, Mena G, Tandon P, Hottowy P, Sher A, Litke A, Mitra S, Chichilnisky EJ. 2019. Optimization of electrical stimulation for a high-fidelity artificial retina. In *9th International IEEE/EMBS Conference on Neural Engineering (NER)*, pp. 714–718. March 20–23.
- Silveira LCL, Heywood CA, Cowey A. 1987. Contrast sensitivity and visual-acuity of the pigmented rat determined electrophysiologically. *Vision Res* **27**: 1719–1731. doi:10.1016/0042-6989(87)90101-5
- Sim SL, Szalewski RJ, Johnson LJ, Akah LE, Shoemaker LE, Thoreson WB, Margalit E. 2014. Simultaneous recording of mouse retinal ganglion cells during epiretinal or subretinal stimulation. *Vision Res* **101**: 41–50. doi:10.1016/j.visres.2014.05.005
- Smith W, Assink J, Klein R, Mitchell P, Klaver CC, Klein BE, Hofman A, Jensen S, Wang JJ, de Jong PT. 2001. Risk factors for age-related macular degeneration: pooled findings from three continents. *Ophthalmology* **108**: 697–704.
- Stingl K, Bartz-Schmidt KU, Gekeler F, Kusnyerik A, Sachs H, Zrenner E. 2013. Functional outcome in subretinal electronic implants depends on foveal eccentricity. *Invest Ophthalmol Vis Sci* **54**: 7658–7665.
- Stingl K, Bartz-Schmidt KU, Besch D, Chee CK, Cottrill CL, Gekeler F, Groppe M, Jackson TL, MacLaren RE, Koitschev A, et al. 2015. Subretinal visual implant Alpha IMS—clinical trial interim report. *Vision Res* **111**: 149–160. doi:10.1016/j.visres.2015.03.001
- Stingl K, Schippert R, Bartz-Schmidt KU, Besch D, Cottrill CL, Edwards TL, Gekeler F, Greppmaier U, Kiel K, Koitschev A, et al. 2017. Interim results of a multicenter trial with the new electronic subretinal implant Alpha AMS in 15 patients blind from inherited retinal degenerations. *Front Neurosci* **11**: 445. doi:10.3389/fnins.2017.00445
- Thibos LN, Levick WR. 1983. Bimodal receptive fields of cat retinal ganglion cells. *Vision Res* **23**: 1561–1572. doi:10.1016/0042-6989(83)90170-0
- Tochitsky I, Polosukhina A, Degtyar VE, Gallerani N, Smith CM, Friedman A, Van Gelder RN, Trauner D, Kaufner D, Kramer RH. 2014. Restoring visual function to blind mice with a photoswitch that exploits electrophysiological remodeling of retinal ganglion cells. *Neuron* **81**: 800–813.
- Wandell B. 1995. *Foundations of vision*. Sinauer Associates, Sunderland, MA.
- Wang BY, Chen ZC, Bhuckory M, Huang T, Shin A, Zuckerman V, Ho E, Rosenfeld E, Galambos L, Kamins T, et al. 2022. Electronic photoreceptors enable prosthetic visual acuity matching the natural resolution in rats. *Nat Commun* **13**: 6627.
- Wässle H. 2004. Parallel processing in the mammalian retina. *Nat Rev Neurosci* **5**: 747–757. doi:10.1038/nrn1497
- Weitz AC, Nanduri D, Behrend MR, Gonzalez-Calle A, Greenberg RJ, Humayun MS, Chow RH, Weiland JD. 2015. Improving the spatial resolution of epiretinal implants by increasing stimulus pulse duration. *Sci Transl Med* **7**: 318ra203. doi:10.1126/scitranslmed.aac4877
- Werginz P, Benav H, Zrenner E, Rattay F. 2015. Modeling the response of ON and OFF retinal bipolar cells during electric stimulation. *Vision Res* **111**: 170–181.
- Werginz P, Wang B-Y, Chen ZC, Palanker D. 2020. On optimal coupling of the “electronic photoreceptors” into the degenerate retina. *J Neural Eng* **17**: 045008.
- Wong WL, Su XY, Li X, Cheung CMG, Klein R, Cheng CY, Wong TY. 2014. Global prevalence of age-related macular degeneration and disease burden projection for 2020 and 2040: a systematic review and meta-analysis. *Lancet Glob Health* **2**: E106–E116.
- Woodburn KW, Engelman CJ, Blumenkranz MS. 2002. Photodynamic therapy for choroidal neovascularization: A review. *Retina* **22**: 391–405. doi:10.1097/00006982-200208000-00001
- Yanovitch L, Raz-Prag D, Hanein Y. 2022. A new high-resolution three-dimensional retinal implant: system design and preliminary human results. bioRxiv doi:10.1101/2022.09.14.507901
- Zrenner E, Bartz-Schmidt KU, Benav H, Besch D, Bruckmann A, Gabel VP, Gekeler F, Greppmaier U, Harscher A, Kibbel S, et al. 2011. Subretinal electronic chips allow blind patients to read letters and combine them to words. *Proc Biol Sci* **278**: 1489–1497. doi:10.1098/rspb.2010.1747